Article

The Canted Antiferromagnetic Approach to Single-Chain Magnets

Kevin Bernot, Javier Luzon, Roberta Sessoli, Alessandro Vindigni, Julien Thion, Sbastien Richeter, Dominique Leclercq, Joulia Larionova, and Arie van der Lee

J. Am. Chem. Soc., **2008**, 130 (5), 1619-1627 • DOI: 10.1021/ja0751734

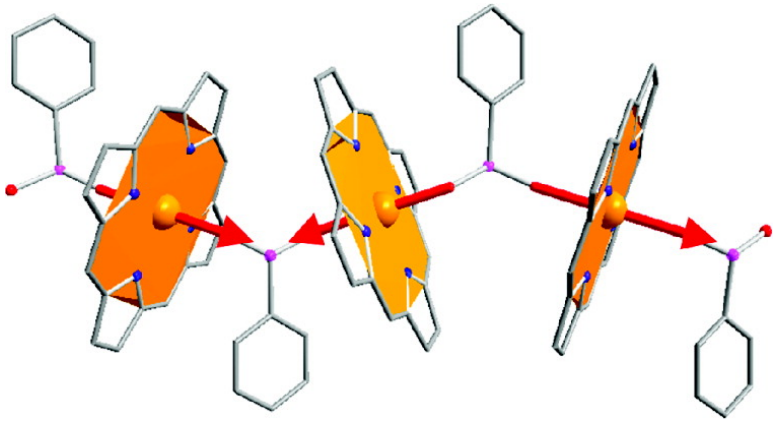

More About This Article

Additional resources and features associated with this article are available within the HTML version:

- Supporting Information
- Links to the 9 articles that cite this article, as of the time of this article download
- Access to high resolution figures
- Links to articles and content related to this article
- Copyright permission to reproduce figures and/or text from this article

View the Full Text HTML

J|A|C|S
ARTICLES
Published on Web 01/15/2008

The Canted Antiferromagnetic Approach to Single-Chain Magnets

Kevin Bernot,[†,‡] Javier Luzon,[†] Roberta Sessoli,*[,†] Alessandro Vindigni,[§] Julien Thion,[||] Sébastien Richeter,[||] Dominique Leclercq,[||] Joulia Larionova,[||] and Arie van der Lee[⊥]

INSTM Research Unit-Dipartimento di Chimica, Università di Firenze, via della Lastruccia 3, 50019 Sesto Fiorentino, Firenze, Italy, Sciences Chimiques de Rennes − Equipe "Matériaux Inorganiques: Chimie Douce et Réactivité" UMR CNRS-INSA 6226, INSA, 20 Avenue des buttes de Coësmes, 35043 Rennes, France, Laboratorium für Festkörperphysik, Wolfgang-Pauli-Strasse 16 ETH Hönggerberg, CH-8093 Zürich, Switzerland, Institut Charles Gerhardt Montpellier, UMR 5253 CNRS-UM2-ENSCM-UM1, Chimie Moléculaire et Organisation du Solide, Université Montpellier II, Place E. Bataillon, 34095 Montpellier cedex 5, France, and Institut Européen des Membranes (IEM), UMR 5635, 34095 Montpellier cedex 5, France

Received July 31, 2007; E-mail: roberta.sessoli@unifi.it

Abstract: The reaction of manganese(III) acetate *meso*-tetraphenylporphyrin with phenylphosphinic acid provides the one-dimensional compound of formula $[Mn(TPP)O_2PHPh]\cdot H_2O$, which crystallizes in the monoclinic *C*2/*c* space group. The chain structure is generated by a glide plane resulting in Jahn−Teller elongation axes of the Mn^{III} octahedra that alternate along the chain. The phenylphosphinate anion transmits a sizable antiferromagnetic exchange interaction that, combined with the easy axis magnetic anisotropy of the Mn^{III} sites, gives rise to a canted antiferromagnetic arrangement of the spins. The static single-crystal magnetic properties have been analyzed with a classical Monte Carlo approach, and the best fit parameters for the exchange and single ion anisotropy are $J = -0.68(4)$ K and $D = -4.7(2)$ K, respectively (using the $-2JS_iS_j$ formalism for the exchange). Below 5 K the single-crystal dynamics susceptibility reveals a frequency-dependent out-of-phase signal typical of single-chain magnets. The extracted relaxation time follows the Arrhenius law with $\Delta = 36.8$ K. The dynamic behavior has been rationalized and correlated to geometrical parameters of the structure. The contribution of the correlation length to the energy barrier has been investigated, and it has been found that the characteristic length that dominates the dynamics strongly exceeds the correlation length estimated from magnetic susceptibility.

Introduction

Molecule-based nanostructures presenting magnetic hysteresis at low temperature without undergoing three-dimensional magnetic ordering have provided a benchmark for the investigation of the dynamics of the magnetization at the nanoscale level,[1,2] including the coexistence of classic and quantum effects.[3−6] The most widely investigated systems are polynuclear clusters behaving like magnets, i.e., single-molecule magnets (SMM),[2,7−11] but recently 1d structures have been demonstrated to be an alternative route to obtain magnetic memory of molecular nature.[12] These systems have been named in analogy single-chain magnets (SCM).[13,14] The thermal equilibrium spin dynamics of quasi 1d magnetic systems close to the ordering temperature has been widely investigated in the past, both from the experimental and theoretical point of view, in particular in the frame of soliton excitations.[15] More recently however, thanks to the molecular approach, it has been possible to synthesize

† Università di Firenze.
‡ Sciences Chimiques de Rennes.
§ Laboratorium für Festkörperphysik.
|| Université Montpellier II.
⊥ Institut Européen des Membranes (IEM).

(1) Gatteschi, D.; Sessoli, R.; Villain, J. *Molecular Nanomagnets*; Oxford University Press: Oxford, UK, 2006.
(2) Gatteschi, D.; Sessoli, R. *Angew. Chem., Int. Ed.* **2003**, *42*, 268−297.
(3) Thomas, L.; Lionti, F.; Ballou, R.; Gatteschi, D.; Sessoli, R.; Barbara, B. *Nature* **1996**, *383*, 145−147.
(4) Friedman, J. R.; Sarachik, M. P.; Tejada, J.; Ziolo, R. *Phys. Rev. Lett.* **1996**, *76*, 3830−3833.
(5) Wernsdorfer, W.; Sessoli, R. *Science* **1999**, *284*, 133−135.
(6) Hill, S.; Edwards, R. S.; Aliaga-Alcalde, N.; Christou, G. *Science* **2003**, *302*, 1015−1018.
(7) Caneschi, A.; Gatteschi, D.; Sessoli, R.; Barra, A.-L.; Brunel, L. C.; Guillot, M. *J. Am. Chem. Soc.* **1991**, *113*, 5873−5874.
(8) Sessoli, R.; Tsai, H. L.; Schake, A. R.; Wang, S.; Vincent, J. B.; Folting, K.; Gatteschi, D.; Christou, G.; Hendrickson, D. N. *J. Am. Chem. Soc.* **1993**, *115*, 1804−16.
(9) Sessoli, R.; Gatteschi, D.; Caneschi, A.; Novak, M. A. *Nature* **1993**, *365*, 141−3.
(10) Christou, G.; Gatteschi, D.; Hendrickson, D. N.; Sessoli, R. *MRS Bull.* **2000**, *25*, 66−71.
(11) Milios, C. J.; Vinslava, A.; Wernsdorfer, W.; Moggach, S.; Parsons, S.; Perlepes, S. P.; Christou, G.; Brechin, E. K. *J. Am. Chem. Soc.* **2007**, *129*, 2754−2755.
(12) Caneschi, A.; Gatteschi, D.; Lalioti, N.; Sangregorio, C.; Sessoli, R.; Venturi, G.; Vindigni, A.; Rettori, A.; Pini, M. G.; Novak, M. A. *Angew. Chem., Int. Ed.* **2001**, *40*, 1760−1763.
(13) Clerac, R.; Miyasaka, H.; Yamashita, M.; Coulon, C. *J. Am. Chem. Soc.* **2002**, *124*, 12837−12844.
(14) Coulon, C.; Miyasaka, H.; Clerac, R. *Structure and Bonding*; Springer: Berlin, 2006; Vol. 122, pp 163−206.

chain compounds where the strong easy axis magnetic anisotropy is combined with a negligible interchain interaction. This has resulted in a slow dynamics of the magnetization out of the thermal equilibrium of pure 1d character with no evidence of 3d magnetic order. The spin dynamics is driven by thermal activated jumps of the spin orientations, described in first approximation by the model developed in the sixties by the Nobel Laureate R. J. Glauber.[16]

Following the observation of SCM behavior in a molecular one-dimensional structure alternating $Co^{II}(hfac)_2$ moieties and nitronyl-nitroxide radicals,[12,17] several compounds presenting SCM behavior have been synthesized[13,18−21] and extensively studied[22−25] including more exotic structures, such as strings of cobalt atoms on Pt terraces.[26]

The two requirements needed to observe the SCM behavior consist generally in a strong easy axis anisotropy and strong intrachain interactions with negligible interchain ones. As the dynamics is directly related to the energy cost to nucleate an infinitely narrow domain wall along the chain, the main parameter to be optimized is the intrachain exchange interaction.

Ferromagnetic interactions, relying on the orthogonality of the magnetic orbitals of the interacting building blocks, are significantly weaker and less common than antiferromagnetic ones.[27,28] The latter have been exploited in the case of interactions between different spins to yield ferrimagnetic SCM.

Antiferromagnetic interactions between like spins in principle can also be exploited to give SCM provided that magnetic anisotropy is present and the easy axes are not collinear. In fact in this case the AF-coupled moments make an angle different from 180°, resulting in an uncompensated moment. It is very frequent in molecular systems that the symmetry on the metal site is lower than that of the crystal space group and the 1d structure is generated by either a glide plane or a screw axis, thus inducing non-collinearity of the anisotropy axes.

Among the possible spin carriers that exhibit easy axis magnetic anisotropy Mn^{III} ions are the most commonly employed given its large spin, $S = 2$, and the Jahn−Teller elongation of the coordination octahedron that induces large single ion easy axis anisotropy. Previously, some of us showed that canted AF chains are formed by Mn^{III} spins in $[Mn(cyclam)SO_4]ClO_4 \cdot H_2O$ (where cyclam is 1,4,8,11-tetraazacyclotetradecane). Sizable interchain interactions of the uncompensated moments trigger in this compound a transition to 3d magnetic order.[29] We proposed that by reducing the interchain interactions a change from 3d order to 1d slow relaxation could be observed.

We have now found that indeed the substitution of cyclam ligands and sulfate anions with porphyrin (*meso*-tetraphenylporphyrin = TPP) and phenylphosphinate, respectively, to obtain the compound of formula $[Mn(TPP)O_2PHPh] \cdot H_2O$ has provided an example of canted AF structure that shows SCM behavior. This behavior has previously been observed for a 1d Co^{II} antiferromagnet presenting canted magnetic structure.[30] However the orbital degeneracy of the metal ion did not allow establishing clear magneto−structural correlations. These last are very important as they can provide hints to develop a canted antiferromagnetic strategy to SCM. On the contrary $[Mn(TPP)O_2PHPh] \cdot H_2O$ contains the orbitally nondegenerate Mn^{III} ions, for which extensive structural magnetic correlations are available.[31]

We want to show here that $[Mn(TPP)O_2PHPh] \cdot H_2O$ is a textbook example of SCM which can be used as a model for many new materials. In fact it represents the first system comprising only one type of spin and one type of exchange interaction, allowing us to simulate with one model both static and dynamic properties on the whole investigated temperature

(15) (a) Villain, J. *Physica B* **1975**, *79*, 1. (b) Smit, H. H. A.; de Groot, H. J. M.; Elmassalami, M.; Thiel, R. C.; de Jongh, L. J. *Physica B* **1989**, *154*, 237. (c) Elmassalami, M.; de Jongh, L. J. *Physica B* **1989**, *154*, 254. (d) Elmassalami, M.; Smit, H. H. A.; Thiel, R. C.; de Jongh, L. J. *Physica B* **1989**, *154*, 267. (e) Mikeska, H. J.; M. Steiner, M. *Adv. Phys.* **1991**, *40*, 191−356. (f) Nagler, S. E.; Buyers, W. J. L.; Armstrong, R. L.; Briat, B.; *Phys. Rev. B: Condens. Mater. Phys.* **1983**, *28*, 3873.

(16) Glauber, R. J. *J. Math. Phys.* **1963**, *4*, 294−307.

(17) Caneschi, A.; Gatteschi, D.; Lalioti, N.; Sangregorio, C.; Sessoli, R.; Venturi, G.; Vindigni, A.; Rettori, A.; Pini, M. G.; Novak, M. A. *Europhys. Lett.* **2002**, *58*, 771−777.

(18) (a) Lescouezec, R.; Vaissermann, J.; Ruiz-Perez, C.; Lloret, F.; Carrasco, R.; Julve, M.; Verdaguer, M.; Dromzee, Y.; Gatteschi, D.; Wernsdorfer, W. *Angew. Chem., Int. Ed.* **2003**, *42*, 1483−1486. (b) Pardo, E.; Ruiz-Garcia, R.; Lloret, F.; Faus, J.; Julve, M.; Journaux, Y.; Delgado, F.; Ruiz-Perez, C. *Adv. Mater.* **2004**, *16*, 1597. (c) Toma, L. M.; Lescouezec, R.; Pasan, J.; Ruiz-Perez, C.; Vaissermann, J.; Cano, J.; Carrasco, R.; Wernsdorfer, W.; Lloret, F.; Julve, M. *J. Am. Chem. Soc.* **2006**, *128*, 4842−4853.

(19) (a) Miyasaka, H.; Clerac, R.; Mizushima, K.; Sugiura, K.; Yamashita, M.; Wernsdorfer, W.; Coulon, C. *Inorg. Chem.* **2003**, *42*, 8203−8213. (b) Miyasaka, H.; Madanbashi, T.; Sugimoto, K.; Nakazawa, Y.; Wernsdorfer, W.; Sugiura, K.; Yamashita, M.; Coulon, C.; Clerac, R. *Chem.−Eur. J.* **2006**, *12*, 7029−7040. (c) Lecren, L.; Wernsdorfer, W.; Li, Y. G.; Vindigni, A.; Miyasaka, H.; Clerac, R. *J. Am. Chem. Soc.* **2007**, *129*, 5045−5051.

(20) (a) Bogani, L.; Sangregorio, C.; Sessoli, R.; Gatteschi, D. *Angew. Chem., Int. Ed.* **2005**, *44*, 5817−5821. (b) Bernot, K.; Bogani, L.; Caneschi, A.; Gatteschi, D.; Sessoli, R. *J. Am. Chem. Soc.* **2006**, *128*, 7947−7956. (c) Bernot, K.; Bogani, L.; Sessoli, R.; Gatteschi, D. *Inorg. Chim. Acta* **2007**, *360*, 3807−3812.

(21) (a) Costes, J. P.; Clemente-Juan, J. M.; Dahan, F.; Milon, J. *Inorg. Chem.* **2004**, *43*, 8200−8202. (b) Liu, T. F.; Fu, D.; Gao, S.; Zhang, Y. Z.; Sun, H. L.; Su, G.; Liu, Y. J. *J. Am. Chem. Soc.* **2003**, *125*, 13976−13977. (c) Kajiwara, T.; Nakano, M.; Kaneko, Y.; Takaishi, S.; Ito, T.; Yamashita, M.; Igashira-Kamiyama, A.; Nojiri, H.; Ono, Y.; Kojima, N. *J. Am. Chem. Soc.* **2005**, *127*, 10150−10151. (d) Balanda, M.; Rams, M.; Nayak, S. K.; Tomkowicz, Z.; Haase, W.; Tomala, K.; Yakhmi, J. V. *Phys. Rev. B: Condens. Mater. Phys.* **2006**, *74*, art. no. 224421. (e) Bai, Y. L.; Tao, J.; Wernsdorfer, W.; Sato, O.; Huang, R. B.; Zheng, L. S. *J. Am. Chem. Soc.* **2006**, *128*, 16428−16429.

(22) Evangelisti, M.; Bartolome, J.; De Jongh, L. J.; Filoti, G. *Phys. Rev. B: Condens. Mater. Phys.* **2002**, *66*, art. no. 144410.

(23) (a) Mito, M.; Shindo, N.; Tajiri, T.; Deguchi, H.; Takagi, S.; Miyasaka, H.; Yamashita, M.; Clerac, R.; Coulon, C. *J. Magn. Magn. Mater.* **2004**, *272−276*, 1118−1119. (b) Coulon, C.; Clerac, R.; Lecren, L.; Wernsdorfer, W.; Miyasaka, H. *Phys. Rev. B: Condens. Mater. Phys.* **2004**, *69*, art. no. 132408. (c) Wernsdorfer, W.; Clerac, R.; Coulon, C.; Lecren, L.; Miyasaka, H. *Phys. Rev. Lett.* **2005**, *95*, art. no 237203. (d) Saitoh, A.; Miyasaka, H.; Yamashita, M.; Clerac, R. *J. Mater. Chem.* **2007**, *17*, 2002−2012.

(24) (a) Bogani, L.; Caneschi, A.; Fedi, M.; Gatteschi, D.; Massi, M.; Novak, M. A.; Pini, M. G.; Rettori, A.; Sessoli, R.; Vindigni, A. *Phys. Rev. Lett.* **2004**, *92*, art. no. 207204. (b) Vindigni, A.; Rettori, A.; Bogani, L.; Caneschi, A.; Gatteschi, D.; Sessoli, R.; Novak, M. A. *Appl. Phys. Lett.* **2005**, *8*, art. no. 073102. (c) Bogani, L.; Sessoli, R.; Pini, M. G.; Rettori, A.; Novak, M. A.; Rosa, P.; Massi, M.; Fedi, M. E.; Giuntini, L.; Caneschi, A.; Gatteschi, D. *Phys. Rev. B: Condens. Mater. Phys.* **2005**, *72*, art. no. 064406. (d) Bogani, L.; Cavigli, L.; Bernot, K.; Sessoli, R.; Gurioli, M.; Gatteschi, D. *J. Mater. Chem.* **2006**, *16*, 2587−2592.

(25) (a) Kishine, J.; Watanabe, T.; Deguchi, H.; Mito, M.; Sakai, T.; Tajiri, T.; Yamashita, M.; Miyasaka, H. *Phys. Rev. B: Condens. Mater. Phys.* **2006**, *74*, art. no. 224419. (b) Oshima, Y.; Nojiri, H.; Asakura, K.; Sakai, T.; Yamashita, M.; Miyasaka, H. *Phys. Rev. B: Condens. Mater. Phys.* **2006**, *73*, art. no. 214435. (c) Mito, M.; Deguchi, H.; Tajiri, T.; Takagi, S.; Yamashita, M.; Miyasaka, H. *Phys. Rev. B: Condens. Mater. Phys.* **2005**, *72*, 144421.

(26) Gambardella, D.; Dallmeyer, H.; Maiti, K.; Malagoli, M. C.; Eberhardt, W.; Kern, K.; Carbone, C. *Nature* **2002**, *416*, 301−304.

(27) Anderson, P. W. *Phys. Rev.* **1959**, *115*, 2.

(28) Kahn, O. *Molecular Magnetism*; VCH: Weinheim, 1993.

(29) Mossin, S.; Weihe, H.; Sorensen, H. O.; Lima, N.; Sessoli, R. *Dalton Trans.* **2004**, 632−639.

(30) (a) Sun, Z.-M.; Prosvirin, A. V.; Zhao, H.-H.; Mao, J.-G.; Dunbar, K. R. *J. Appl. Phys.* **2005**, 97, 10B305. (b) Palii, A. V.; Ostrovsky, S. M.; Klokishner, S. I.; Reu, O. S.; Sun, Z. M.; Prosvirin, A. V.; Zhao, H. H.; Mao, J. G.; Dunbar, K. R. *J. Phys. Chem. A* **2006**, *110*, 14003−14012.

(31) (a) Mossin, S.; Sorensen, H. O.; Weihe, H.; Glerup, J.; Sotofte, I. *Inorg. Chim. Acta* **2005**, *358*, 1096−1106. (b) Tregenna-Piggott, P. L. W.; Weihe, H.; Barra, A. L. *Inorg. Chem.* **2003**, *42*, 8504−8508. (c) Mossin, S.; Weihe, H.; Barra, A. L. *J. Am. Chem. Soc.* **2002**, *124*, 8764−8765. (d) Krzystek, J.; Telser, J.; Pardi, L. A.; Goldberg, D. P.; Hoffman, B. M.; Brunel, L. C. *Inorg. Chem.* **1999**, *38*, 6121−6129. (e) Barra, A. L.; Gatteschi, D.; Sessoli, R.; Abbati, G. L.; Cornia, A.; Fabretti, A. C.; Uytterhoeven, M. G. *Angew. Chem., Int. Ed. Engl.* **1997**, *36*, 2329−2331.

range. This has provided an unprecedented level of characterization among SCM, which has confirmed the contribution of the single ion axis anisotropy and of the exchange correlation length to the energy barrier that hampers the reversal of the magnetization. More relevant is the finding that the correlation length that determines the time scale of the relaxation cannot be directly estimated from the temperature dependence of the susceptibility and a more detailed analysis, like the one presented here, becomes necessary.

Experimental Section

Synthesis. All of the chemical reagents used in these experiments were analytical grade. The precursor [Mn(TPP)OAc] was prepared as already described.[32]

Synthesis of [Mn(TPP)O_2PHPh]·H_2O. The manganese(III) acetate *meso*-tetraphenylporphyrin complex [Mn(TPP)OAc] (0.73 g, 1 mmol) and phenylphosphinic acid were stirred in refluxing ethanol (30 mL) for 16 h. After evaporation of the solvent and precipitation from dichloromethane/pentane (20/250 mL), 0.72 g of a dark-purple powder was obtained (89% yield). A slow diffusion of the ethanolic solution of the powder with water leads to formation of single crystals of formula [Mn(TPP)O_2PHPh]·H_2O.

IR (KBr disc) ν (cm^{-1}): 2306w (P−H), 1596 m (C═N), 1178 m (PO_2), 1013 s, 802 m, 754 m, 705 m.

UV−visible (in CH_2Cl_2), λ_{nm} (ϵ $L{\cdot}mol^{-1}{\cdot}cm^{-1}$): 376 (53600), 389 (47500), 477 (89300), 529 (5700), 577 (10800), 613 (10500).

FAB^+ MS: Calcd for $C_{50}H_{34}N_4O_2PMn$: 808.74, found: 809.

Elemental Anal. Calcd (%) for $C_{50}H_{34}N_4O_2PMn{\cdot}H_2O$: C, 72.64; H, 4.39; N, 6.78; P, 3.75; Mn, 6.64. Found: C, 72.30; H, 4.43; N, 6.54; P, 3.91; Mn, 6.41.

X-ray Crystallography and Structure Solution. Data collection was performed at 173 K on an Oxford-Diffraction Xcalibur-I single crystal diffractometer using graphite-monochromatized Mo Kα radiation (λ = 0.71073 Å). A total of 1193 frames were collected in the ω-scan mode. The three-dimensional structure was solved in the monoclinic space group *C*2/*c* (no. 15) by using ab initio methods with the recently discovered charge-flipping algorithm.[33] Hydrogen atoms were found from difference Fourier maps, and their positions were optimized using an initial refinement with soft restraints on the bonds and angles to regularize their geometry. The P−H group was found to be disordered over two positions with equal occupation probabilities. The structural refinements were performed with the CRYSTALS package[34] on F_{obs} using reflections with $I > 2\,\sigma(I)$. Details about the data collection and refinement can be found in Table 1.

Physical Measurements. IR spectra were recorded on a Thermo Nicolet Avatar 320 spectrometer with a 4 cm^{-1} resolution in KBr disk. UV−vis spectra were recorded in CH_2Cl_2 solution on a Perkin-Elmer Lambda 35 spectrometer. Elemental analyses were performed by the Service Central d'Analyse (CNRS, Vernaison, France). Magnetic susceptibility data were collected with a Quantum Design MPMS-XL SQUID magnetometer working in the temperature range of 1.8−300 K and the magnetic field range of 0−50 kOe. Powder measurements were performed on pellets in order to avoid orientation under field of these very anisotropic materials. *Direct Current* (*DC*) single crystal measurements were performed on three iso-oriented crystals in order to maximize the signal by using a laboratory-made susceptometer based on the Oxford Instruments MAGLAB 2000 platform[35] for frequencies above 200 Hz and a Quantum Design MPMS-XL SQUID for the lower ones.

Table 1. Crystallographic Data for **1**

formula sum	$C_{100}H_{72}Mn_2N_8O_6P_2$
formula weight crystal system	1653.48 monoclinic
space group	*C*12/*c*1 (no. 15)
unit cell dimensions	
a/Å	23.1760(10)
b/Å	13.1670(8)
c/Å	12.9210(8)
β/(deg)	90.623(4)
cell volume/$Å^3$	3942.7(4)
Z	2
density, calculated/ $g{\cdot}cm^{-3}$	1.393
λ/Å	0.710730
T/K	175
total no. reflections measured	67833
total no. independent reflections	3377
$R_F(1)^a$	0.07384
$R_F(2)$	0.0352
$wR(1)^a$	0.0571
$wR(2)^a$	0.0393

[a] $R_F(1)$ and wR(1) are based on all independent reflections, whereas $R_F(2)$ and wR(2) are based on observed reflections only.

Results

Synthesis and Crystal Structure. The synthesis of the complex [Mn(TPP)O_2PHPh]·H_2O was realized in one step starting from the manganese(III) acetate *meso*-tetraphenylporphyrin complex [Mn^{III}(TPP)OAc].[32] This complex was treated in ethanol with phenylphosphinic acid under reflux in order to exchange the axial acetate ligand by a phenylphosphinate anion. The crude complex was obtained as a dark-purple powder in 89% yield (Figure S1 of Supporting Information, SI). The infrared spectrum of this complex shows the strong absorption band located at ν = 1178 cm^{-1}, characteristic of the $-PO_2$ stretching vibrations.[36]

Crystals of the complex [Mn(TPP)O_2PHPh]·H_2O suitable for a structural X-ray analysis were obtained by slow diffusion of water into an ethanol solution of the powder. The asymmetric unit cell contains one centrosymmetric [Mn(TPP)O_2PHPh] with Mn at the special Wyckoff position (4*a*) of the monoclinc *C*2/*c* space group. Each manganese atom is surrounded by the four nitrogen atoms from TPP ligands and by two oxygen atoms of two bridged phenylphosphinato ligands in *mer* conformation forming a slightly distorted octahedral environment, as shown in Figure 1.

The Mn(1)−N(20) and Mn(1)−N(8) distances are respectively equal to 2.020(2) Å and 2.018(1) Å and the Mn(1)−O(2) distance is 2.155(1) Å showing the presence of Jahn−Teller elongation of the coordination octahedron. The O(2)−Mn(1)−O(2) angle is 180° due to the symmetry, and no deformation of the porphyrin macrocycle is observed. The Mn(1)−O(2) direction forms an angle of only 1.1(1)° with the normal to the Mn−porphyrin plane. The Mn−porphyrin complexes form via the phosphinate ligands infinite $[Mn{-}O{-}P{-}O]_\infty$ zigzag chains along the crystallographic *c*-axis (Figure 1) generated by the glide plane symmetry element (x, $-y$, $z + 1/2$) of the *C*2/*c* space group.

(32) (a) Adler, A. D.; Longo, F. R.; Kampas, F.; Kim, J. *Inorg. Nucl. Chem.* **1970**, *32*, 2443−2445. (b) Buchler, J. W. In *The Porphyrins*; Dolphin, D., Ed.; Academic Press: New York, 1979.
(33) (a) Palatinus, L.; Chapuis, C. *J. Appl. Crystallogr.* **2007**, *40*, 786−790. (b) Oszlányi, G.; Süto, A.; Czugler, M.; Párkányi, L. *J. Am. Chem. Soc.* **2006**, *128*, 8392−8393.
(34) Betteridge, P. W.; Carruthers, J. R.; Cooper, R. I.; Prout, K.; Watkin, D. J. *J. Appl. Crystallogr.* **2003**, *36*, 1487.
(35) Midollini, S.; Oriandini, A.; Rosa, P.; Sorace, L. *Inorg. Chem.* **2005**, *44*, 2060−2066.
(36) Nakamoto, K *Infrared and Raman Spectra of Inorganic and Coordination Compounds*, 2nd ed.; Wiley-Interscience: New York, 1970.

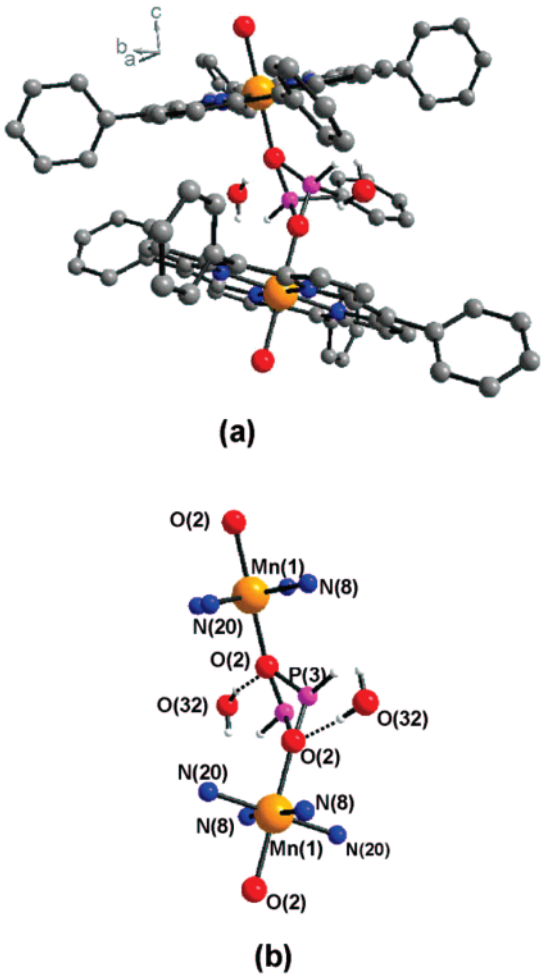

Figure 1. (a) Two MnTPP complexes linked by the phenylphosphinato bridge (H's, except PH and H_2O, omitted for clarity); (b) Detailed view of the inorganic backbone (C's and H's, except PH and H_2O, omitted for clarity). Note that the P(3)H and H_2O(32) positions are occupied for 50% only. Color scheme: Mn, orange; P, pink; O, red; N, blue; C, gray; H, white.

Two P(3)−H(36) positions with an occupation probability of 0.5 each and related by a two-fold symmetry axis parallel to the *b*-axis appear along the chain. The random distribution of the position of the P−H group along the chain indicates that the 1d polymer is atactic. The water molecules are also at an occupation probability of 0.5 and are situated in the interchain space; they are linked randomly by means of a hydrogen bond (2.728(7) Å for O(32)···O32) to one of the oxygen atoms of the phenylphosphinate ligands at the farther position to the P−H group. This phenomenon also explains the bad definition on the position of the phenyl groups on the phosphorus atom. Consequently, the phosphinate bridging ligand forms two kinds of bent interactions with the manganese atom with shorter (1.4611(14) Å) and longer (1.5873(15) Å) P−O linkages. The respective Mn(1)−O(2)−P(3) angles are equal to 171.94(10)° and 131.22(9)° (Table 2). The O(2)−P(3)−O(2) angle is equal to 114.07(10)°. The normal of the porphyrin cycle forms an angle of 21.01° with the *c*-axis, and two consecutive N_4 equatorial basal planes form an angle of 34.6°. The shortest distance measured between two neighboring Mn^{III} centers along the chain is 6.460(1) Å (Table 2). The crystallographic packing consists in an assembly of parallel zigzag chains in the *bc* plane (Figure S2 of SI). The shortest interchain Mn(1)−Mn(1) distances measured are 13.167(0) and 13.328(0) Å (Table 2). A hexagonal-type arrangement between the chains with an optimized occupation of the space is observed (Figure S3 of SI). Except for the water molecules, which are hydrogen bonded to one phenylphosphinate axial ligands, no solvent is found in the interchain space.

Table 2. Selected Bonds Distances (Å) and Angles (deg) for **1** with the Estimated Standard Deviations in Parentheses

distance	Å	angle	(deg)
Mn(1)−N(20)	2.020(1)	N(20)−Mn(1)−N(20)	179.994
Mn(1)−N(8)	2.018(1)	N(8)−Mn(1)−N(8)	179.994
Mn(1)−O(2)	2.155(1)	N(8)−Mn(1)−N(20)	89.68(6)
O(2)−P(3)	1.461(1)	N(8)−Mn(1)−N(20)	90.32(6)
O(2)−P(3)	1.587(2)	O(2)−Mn(1)−O(2)	179.995
P(3)−H(36)	1.288	O(2)−Mn(1)−N(20)	90.01(5)
P(3)−C(4)	1.861(3)	Mn(1)−O(2)−P(3)	131.22(9)
O(2)−O(32)	2.728(7)	Mn(1)−O(2)−P(3)	171.94(10)
Mn−Mn[a]	6.460(1)	O(2)−P(3)−O(2)	114.07(10)
Mn−Mn[b]	13.167(0)	O(2)−P(3)−C(4)	102.89(7)
Mn−Mn[c]	13.328(0)	O(2)−P(3)−C(4)	108.25(7)

[a] Intrachain, symmetry operation: $x, -y, 1.5 + z$. [b] Interchain, symmetry operation: $x, -1 + y, z$. [c] Interchain, symmetry operation: $-0.5 + x, 0.5 + y, z$.

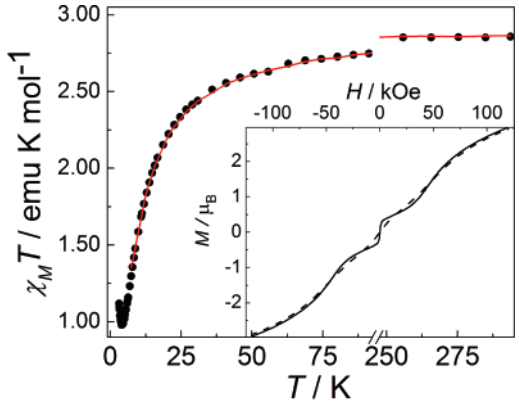

Figure 2. $\chi_M T$ vs T of the powder susceptibility. The red line corresponds to the calculated susceptibility (see text). In the inset the magnetization against field for the powder sample at 1.6 K (full line) and 4 K (dashed line) is reported. The acquisition was made while continuously sweeping at 4 kOe/min.

Magnetic Properties. The temperature dependence of the molar magnetic susceptibility per formula unit in the form $\chi_M T$ for a microcrystalline powder sample is shown in Figure 2. The room-temperature value, 2.92 emu K mol^{-1} is in agreement with the presence of high-spin Mn^{III} ions with $S = 2$ and $g = 1.97$. As the temperature is lowered, $\chi_M T$ decreases to reach a minimum of 0.98 emu K mol^{-1} at 3.9 K and increases at lower temperature. This behavior is typical of antiferromagnetic 1d Mn^{III} structures in the presence of spin canting.[29]

Given the expected magnetic anisotropy of Mn^{III} ion, we have investigated the single-crystal magnetic properties by using a horizontal rotator in the SQUID magnetometer. The angular dependences of the susceptibility measured in the *bc* and *a*c* planes are reported in Figure 3 for two temperatures, 2.5 and 5.5 K, respectively. The whole investigated angular range of the susceptibility is shown in Figures S4 and S5 of SI. The extremes are always found along the same directions, confirming that no significant structural phase transition occurs at low temperature. One of the principal magnetic axes coincides with the *b* crystallographic one, as expected for a monoclinic lattice. The other two magnetic axes determined from the extremes of

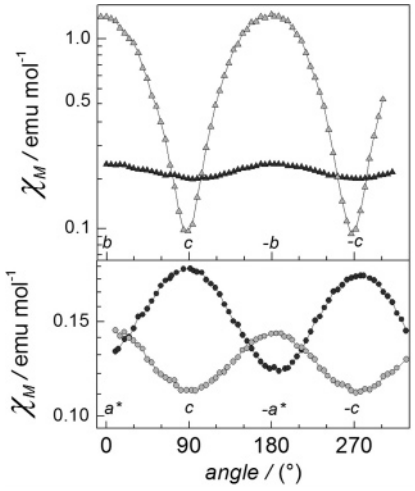

Figure 3. Plot of the molar susceptibility against the rotation angle. Rotation along *a** (top) and *b* (bottom) are depicted for two temperatures, 2.5 K (light gray) and 5.5 K (dark gray).

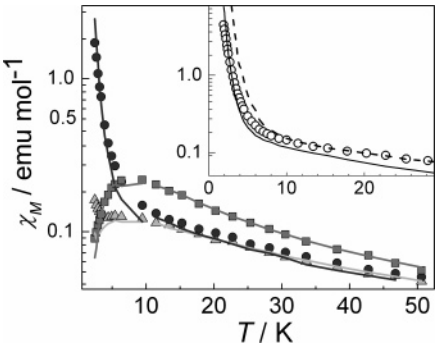

Figure 4. Plot of the molar susceptibility extracted from the rotating crystal measurement versus the temperature with the field (1 kOe) applied along *a* (triangle), *b* (circles), and *c* (squares). Monte Carlo simulations are superimposed. (Inset) Empty circles represent the zero field ac susceptibility (0.1 Hz) along the *b*-axis together with the calculated values with $S = 2$ (full line) and $S = 2.45$ (dashed line) as discussed in the text. The crossover between the two regimes occurs around 10 K and is represented by a break in the lines of the main graph.

the angular dependence of the susceptibility in the *bc* and *ac* planes are found almost to coincide with *a** and *c* axes, even if these results are not symmetry imposed. Given that the β angle is very close to 90° we will name for simplicity the three principal directions for the magnetic anisotropy as *a*, *b*, and *c*.

The temperature dependence of the susceptibility was measured on the single crystal along the three principal axes in a field of 1 kOe (Figure 4). At high temperature, the susceptibility is largest along *c*, this being the closest direction to the easy axis of magnetization of each Mn^{III} center. On the temperature being lowered, the behavior is very different for the three directions. Along the *c* direction the susceptibility goes through a round maximum around 9 K, as expected for an antiferromagnet. Along *b* the susceptibility first increases gradually as the temperature decreases and then a faster increase is observed below ca. 8 K, indicating the presence of a short-range correlation between uncompensated magnetic moments along this direction. A very small increase of the susceptibility with decreasing the temperature (notice the logarithmic scale) is observed along the *a*-axis.

The field dependence of the magnetization was measured on a single crystal at 2.3 K along the three principal directions

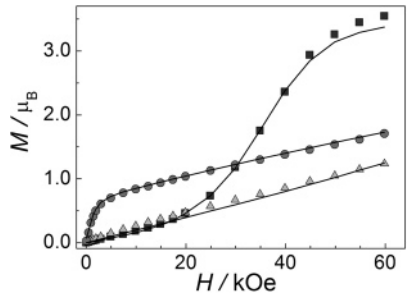

Figure 5. Plot of the magnetization against field for each axis (*a* as triangles, *b* circles, and *c* squares) at $T = 2.3$ K. Monte Carlo calculated values with the best fit parameters discussed in the text are shown as solid lines.

(Figure 5). Along *c* the low-field magnetization is very small but increases abruptly around 35 kOe when the applied field overwhelms the AF interaction mediated by the phosphinate ligand. Along *b* a fast saturation is observed at 2.3 K, with a leveling of the magnetization at ca. 0.8 μ_B, and a slow increase at higher field. This is the typical behavior of weak ferromagnets when the field is applied along the direction of the uncompensated magnetic moments. Along *a* the behavior is linear and very weakly dependent on the temperature in agreement with the susceptibility curve reported in Figure 4. The field dependence of the magnetization performed on the powder sample shows an intermediate behavior between the ones obtained for *c* and *b* orientations (see inset of Figure 2). No opening of a hysteresis cycle was observed at 1.6 K with a sweeping rate of 4 kOe/min.

AC magnetic measurements have been performed on an oriented sample constituted by three aligned single crystals in three principal directions (Figure 6). Temperature dependences of the in-phase, χ', and out-of-phase, χ'', components of the AC susceptibility measured with the frequency varying from 0.1 to 20,000 Hz reveal the typical SCM behavior with frequency-dependent maxima in χ' and χ'', and no evidence of frequency-independent anomalies in χ'', as otherwise observed when 3d ordering occurs. As expected, below 6 K the susceptibility is much stronger along the *b*-axis, and only along this direction is the intensity of χ'' signal comparable with that of χ'. The temperature dependences of the χ' and χ'' components of the AC susceptibility measured on a powder sample are close to what is observed along the *b*-axis and are presented in Figure S6 of SI.

The temperature dependence of the relaxation time, extracted from the maximum of the χ'' vs ω curves assuming $\tau = (\omega_{max})^{-1}$, was fitted with an Arrhenius law, $\tau = \tau_0 \exp(\Delta/k_B T)$, where Δ is the average energy barrier for the reversal of the magnetization, τ_0 is the attempt time, and k_B is the Boltzmann constant. The values of the energy barrier, Δ/k_B, and of the pre-exponential factor τ_0 extracted from the powder sample measurements are equal to 36.8 (±0.6) K and 1.6 (±0.4) × 10^{-10} s, respectively (Figure 7). Single crystal data taken along the *b*-axis are a little noisier but provide similar parameters ($\Delta/k_B = 34.6$ (±0.9) K and $\tau_0 = 3.5$ (±0.5) × 10^{-10} s). The application of a static magnetic field of 1 kOe has no sizable effects on the dynamic parameters (inset of Figure 7).

Information on the distribution of relaxation times can be extracted by plotting χ'' against χ' for each temperature in the

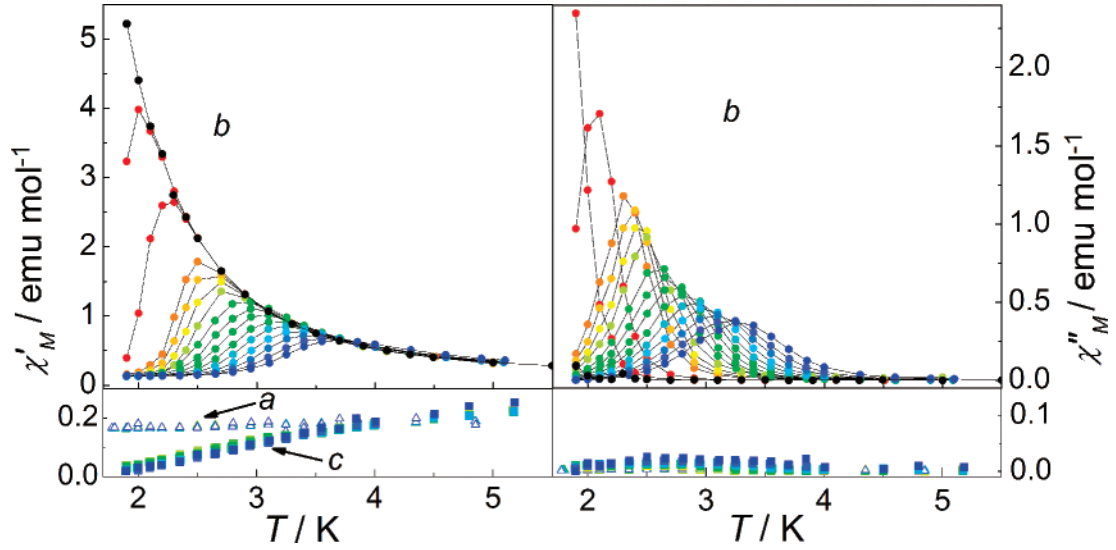

Figure 6. Plot of the real (χ') and imaginary (χ'') molar susceptibility against the temperature measured in zero static field. The measurements were performed with logarithmic spaced frequencies ranging from 4 Hz (red) to 20000 Hz (blue). The black symbols stay for zero field quasi-static susceptibility measured at 0.1 Hz. The crystals were oriented along *a* (open triangles), *b* (circles), and *c* (squares) axis.

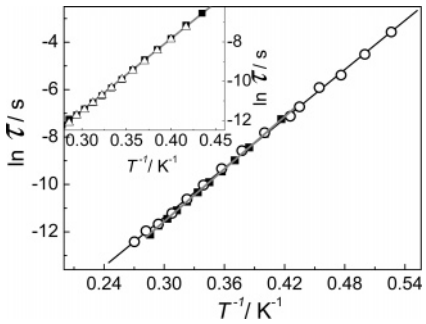

Figure 7. Arrhenius plots and best linear fits for powder (circles, fit as full line) and crystals (squares, fit as gray line). (Inset) Arrhenius plots and best linear fits for powder with zero (solid squares) and 1 kOe static field (triangles).

Argand plot.[37] According to the Debye theory the ideal behavior in the case of a single relaxation time is a semicircle, while a parameter α can be introduced to characterize the distribution of the relaxation time in the sample. In the ideal case α should be zero, but values up to 0.1 are often observed in SMMs and SCMs.[1,38] To allow easy comparison between different temperatures, both χ' and χ'' have been normalized by the isothermal ($\omega \rightarrow 0$) susceptibility, as shown in Figure 8. For the powder sample, the α parameter takes a very low value, 0.014 at 3.2 K, which slowly increases to 0.076 at 2.5 K, confirming the SCM behavior. For single crystal measurements the α value is slightly higher and equal to 0.085 at 3.2 K and 0.1 at 2.5 K. Interestingly the Argand plots show that the first intercept of the semicircle with the *x*-axis, i.e., χ' for $\omega \rightarrow \infty$, occurs at a significantly larger χ' in the powder experiments compared to those in the single crystal ones. This is due to the fast relaxing *a* and *c* components of the magnetization, not present when measuring along *b*.

Discussion

There are several features that make this relatively simple system an ideal candidate to reach an unprecedented level of understanding of the slow dynamics of the magnetization characteristic of SCMs: (i) Given the large separation between the chains induced by the porphyrin ligands, we can in fact neglect interchain interaction; (ii) the large value of the Mn^{III} spin, $S = 2$, allows treating the system as an ensemble of classical spins; (iii) the quenched orbital contribution allows treating the intrachain exchange interaction as isotropic; (iv) the Jahn−Teller elongation of the octahedron around Mn^{III} induces a predictable orientation of the easy axis of the single ion magnetic anisotropy; (v) single crystal data have been collected for both static and dynamic magnetic properties.

Considering the first four points of the previous paragraph, we have performed a classical Monte Carlo study[39] of the static magnetic properties using the following one-dimensional anisotropic Heisenberg Hamiltonian:

$$\mathcal{H} = -2J \sum_k \bar{S}_k \bar{S}_{k+1} + D \sum_k (S_k^{z_k})^2 \qquad (1)$$

where $S = \sqrt{S(S+1)} = \sqrt{2(2+1)}$ is the scaled classical spin, *J* is the isotropic intrachain magnetic interaction, *g* is the gyromagnetic factor, *D* is the uniaxial magnetic anisotropy term for the Mn^{III} ions, and z_k is the single-ion easy anisotropy axis for the *k* Mn^{III} ion, which is expected to coincide with the normal to the porphyrin plane. Given that the chain is generated by a glide plane, two symmetry-related z_k and $z_{k\pm1}$ local axes alternate, as shown in Figure 9.

Both easy anisotropy axes form an angle θ of 21.01° with the *c* crystallographic axis, but they define a plane that does not contain *c*. The projection of these axes on the *a***b* plane forms angles ϕ of ±56.55° with the *a** axis. This results in a very large canting angle, $\delta = 34.6°$, between the two different easy-anisotropy axes. The experimental data of Figures 4 and 5 confirm this picture, with the larger low-temperature susceptibility and fast saturation measured along *b* due to the noncompensation of the antiferromagnetic coupled spins along the chain.

(37) Cole, K. S.; Cole, R. H. *J. Chem. Phys.* **1941**, *9*, 341.
(38) Dekker, C.; Arts, A. F. M.; Wijn, H. W.; van Duyneveldt, A. J.; Mydosh, J. A. *Phys. Rev. B: Condens. Mater. Phys.* **1989**, *40*, 11243.
(39) Metropolis, N.; Rosenbluth, A. W.; Rosenbluth, M. N.; Teller, A. H.; Teller, E. *J. Chem. Phys.* **1953**, *21*, 1087−1092.

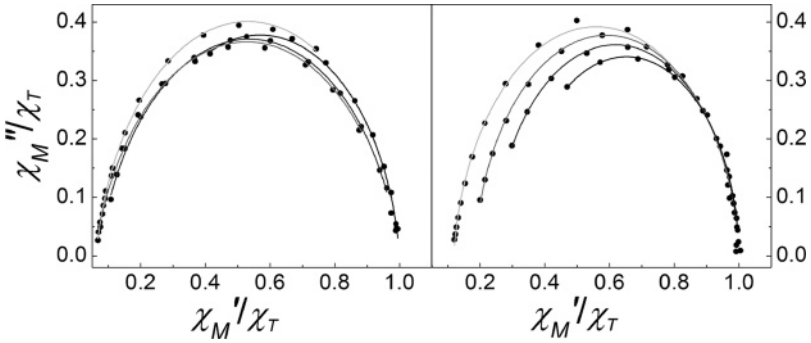

Figure 8. Argand plot of powder sample (right) and crystals oriented with the oscillating field along *b* (left) with most representatives fits reported as lines from $T = 2.3$ K (light gray) up to 3.2 K (dark gray). α values are discussed in the text.

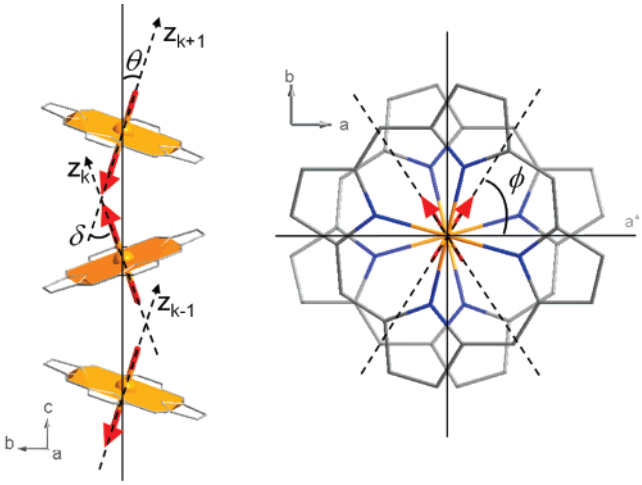

Figure 9. Schematic views along *a* (left) of the chain structure where the local easy axes z_k, normal to the orange equatorial plane, are highlighted. On the right the projection along *c* is shown with the projection of the local easy axes in the *ab* plane represented by the dashed lines. The AF spin structure is shown by red arrows.

Monte Carlo calculations were performed using a single-spin movement Metropolis[39] algorithm with periodic boundary conditions and a size system of $L = 100$ magnetic ions. For computing equilibrium average 5×10^6 Monte Carlo steps per spin were performed after a thermalization of 1×10^6 steps per spin.

Optimized values for the magnetic interaction, $J = 0.68(4)$ K, the axial magnetic anisotropy, $D = -4.7(2)$ K, and the gyromagnetic factor, $g = 1.97(1)$, were obtained by fitting together the magnetic susceptibilities along *a*-, *b*-, *c*-axes above 10 K and the magnetization vs field at 2.3 K along the *a*-, *b*-, and *c*-axes. For the fit of the magnetization data the value used for the scaled classical spin was 2 since at low temperature, when the correlation becomes relevant, $\langle S^2 \rangle$ is closer to S^2 than to $S(S + 1)$.

It is important to notice that taking into account the gradual reduction of the quantum correction on lowering the temperature (the calculated values for the two extremes being reported in the inset of Figure 4) the same set of parameters is able to satisfactorily reproduce the data on the entire temperature and field ranges, including the zero field data of the inset of Figure 4. This rules out the occurrence of 3d magnetic order, contrarily well evident in the less sterically hindered [Mn(cyclam)SO_4]-ClO_4·H_2O compound.[29] The low temperature increase of the susceptibility along *b* is solely due to the 1d short-range order correlation of the rather large uncompensated moments in this strongly canted structure. The low-temperature susceptibility along *a* is estimated to be flat at low temperature, while the experimental data in Figure 4 show a small increase. This discrepancy can be reasonably attributed to an imperfect alignment of the crystal, rather likely for the actual shape of the crystal, rather likely for the actual shape of the crystal, with a resulting small contribution of the diverging *b* component.

It could appear as contradictory that SCM behavior, well described by the Glauber model developed for the Ising chain, can be observed also in presence of isotropic exchange. Indeed it has been shown that, in the presence of Heisenberg interaction and easy axis single ion anisotropy, the domain wall becomes infinitely sharp, i.e., contains only one unit cell, when the ratio $|D/J|$ exceeds 4/3.[40] In the present case, where $|D/J| = 6.9$, this condition is well fulfilled. Therefore, the spins are allowed to point toward a unique direction, and the relaxation time at low temperature is given by:

$$\tau = \frac{\tau_0}{2} \exp(8\beta|J|S^2) \qquad (2)$$

where $\beta = 1/k_B T$ and τ_0 is the relaxation time for one spin in the absence of exchange interactions ($J = 0$). The relaxation in fact involves the nucleation of a domain wall that costs 4 times the nearest neighbor exchange energy.

In the case of an Ising system, on which the Glauber model is based,[16] the spin correlation length ξ diverges at low temperature as $\exp(4\beta|J|S^2)$.[41−43] Therefore, the previous expression can be written as:

$$\tau \propto \tau_0 \xi^2 \qquad (3)$$

This expression has also an intuitive physical interpretation based on the "random walk" theory. In fact at low temperatures an Ising system consists of large spin domains with lengths of the order of the correlation length ξ.[44] The slow relaxation time of the magnetization, τ, is related to the characteristic time for the decay of a domain, that corresponds to the time the domain wall needs to cover the segment of correlated spins. Considering a random walk of the domain walls, i.e., at each step the domain wall has the same probability to go either forward or backward,

(40) (a) Barbara, B. *J. Phys.* **1973**, *34*, 1039. (b) Barbara, B. *J. Magn. Magn. Mater.* **1994**, *129*, 79−86.
(41) Ising, E. *Z. Phys.* **1925**, *31*, 253.
(42) de Jongh, L. J.; Miedema, A. R. *Adv. Phys.* **1974**, *23*, 1.
(43) Steiner, M.; Villain, J.; Windsor, C. G. *Adv. Phys.* **1976**, *25*, 87−209.
(44) Kishine, J.; Watanabe, T.; Deguchi, H.; Mito, M.; Sakai, T.; Tajiri, T.; Yamashita, M.; Miyasaka, H. *Phys. Rev. B: Condens. Mater. Phys.* **2006**, *74*, art. no. 224419.

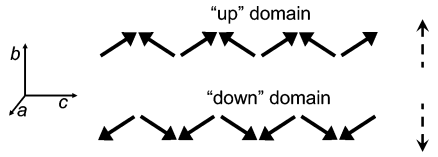

Figure 10. Schematic representation of the projection on the *bc* plane of the two kinds of spin domains. Full arrows: spin projection; dashed arrows: direction of the noncompensated magnetization of the domain.

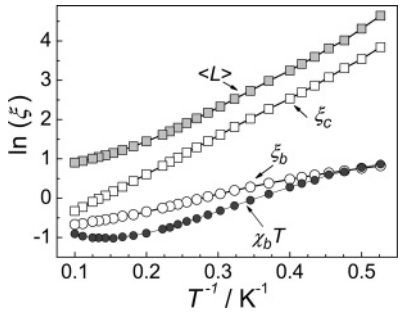

Figure 11. Semilogarithm plot of the correlation length (ξ) versus $1/T$. Classical Monte Carlo simulations along the *b*-axis (empty circles), along the *c*-axis (empty squares), and average length of the spin domains (gray-filled squares). Full circles represents the experimental zero field $\chi_M T$ along the *b*-axis, rescaled to be superimposed to the calculated ξ.

the time for the domain wall to move a length ξ is proportional to $\tau_0\xi^2$, where τ_0 is the characteristic time for a step in the domain wall movement.

It is interesting to stress that only applying a magnetic field along *b* the magnetization component show a complete freezing with just one relaxation time. Intuitively the unique character of the *b* direction can be justified by considering the different effect of the magnetic field on the domains, as schematized in Figure 10. In the absence of a field but at finite temperature, the chain can be regarded as a succession of two types of domains, "up" and "down", with noncompensated magnetization parallel or antiparallel to the *b*-axis, respectively, which are separated by sharp domain walls.

Applying a magnetic field along the *b*-axis the energy of the "up" domains decreases compared to that of the "down" domains. This induces a reduction of the size of "down" domains by moving the domain walls, thus resulting in a slow relaxation of the magnetization. On the contrary, when a magnetic field is applied along *a* or *c*, the field does not change the relative energy of the two types of domains and the relaxation is fast because it does not involve movements of domain walls but rather small reorientations of the spins inside the domains. A formal demonstration of this intuitive result can be obtained through an extension of the original Glauber theory,[16,17] which is reported in the Appendix in SI for the interested readers.

Some considerations about τ_0 are needed to describe the dynamics behavior of this system. It has been assumed that the dynamics of each anisotropic paramagnetic center can be described by a multiphonon Orbach process necessary to overcome the energy barrier generated by the single ion anisotropy.[1,45] Therefore, in the case of this Heisenberg system with strong single-ion uniaxial anisotropy, τ_0 can be rewritten as[14,23b]

$$\tau_0 = \tau_0' \exp(\beta|D|S^2) \quad (4)$$

Since in our system the single-ion easy anisotropy axis of adjacent ions form an angle δ of 34.6°, the *J* value in expression 2 has to be replaced by $J \cos \delta$ if the spins are considered collinear to the easy anisotropy axis, thus yielding:

$$\xi \propto \exp(4\beta S^2|J| \cos \delta) \quad (5)$$

Combining the last expressions we obtain:

$$\tau_0 = \tau_0' \exp(\beta|D|S^2 + 8\beta S^2|J| \cos \delta) = \tau_0' \exp(\beta\Delta) \quad (6)$$

where the energy barrier is formed by the contributions coming from the correlation and the single ion anisotropy:[14,23b]

$$\Delta = 8S^2|J| \cos\delta + |D|S^2 = 2\Delta_\xi + \Delta_{s.i.} \quad (7)$$

Using *J* and *D* values obtained from the Monte Carlo fit we get $\Delta = 37(2)$ K, a value within error co-incident with the experimental one of 36.8 K.

To be more precise the assumption that the spins are aligned along their local anisotropy axis is only valid for $|D/J| \rightarrow \infty$. When this limit is not reached, the energy is minimized with a smaller canting than that expected from structural consideration, as indeed suggested by the magnetization along *b*, which seems to saturate at a value smaller than $4 \sin \theta \sin\phi \approx 1.2\mu_B$. This reduction of the canting, in principle, yields a longer correlation length but the effect on the dynamics is not that straight forward, because it is partially balanced by a reduced contribution of the single ion anisotropy. A comparison of systems with different $|D/J|$ ratio would be necessary to better clarify this point.

Coming back to eq 3 it is interesting to notice that in a non-collinear spin system, like the present one, three different correlation lengths along the chain can be defined, depending on which of the *a*, *b*, and *c* component of the magnetization is considered. In Figure 11 we report the calculated ξ_b and ξ_c for the *b* and *c* component, respectively, using the parameters of the best-fit of the magnetic data. At low temperature they both approach an exponential divergence, but it occurs at much higher temperatures for ξ_c, being *c* closer to the local easy axes. The correlation lengths have been simulated with the expression $\xi = C\exp(\beta\Delta_\xi)$ and ξ_c is found to diverge much faster than ξ_b, with $\Delta_\xi = 9.7$ and 3.4 K, respectively. Similar results are obtained through a Transfer Matrix approach. The MC approach also allows computing the average length $\langle L \rangle$ of the ordered spin domains, introduced in our intuitive description of the relaxation phenomenon. This length coincides with the spin correlation length in an Ising model, where the spins have only one degree of freedom. In our case the domain length is found to be larger than the correlation length, because spins belonging to the same domain still have some degrees of freedom that reduce their correlation. However, at low temperature the two quantities have almost the same Δ_ξ, as demonstrated by the two parallel lines in the semilogarithmic plot of Figure 11. Introducing the value Δ_ξ for the average domain length (9.9 K) in (7) the energy barrier for the dynamics of the magnetization is evaluated to be 38.6 K, close to the experimental value of 36.8 K.

(45) Villain, J.; Hartmann-Boutron, F.; Sessoli, R.; Rettori, A. *Europhys. Lett.* **1994**, *27*, 159−164.

In the 1d ferromagnetic Ising model the correlation length at low temperature can be directly extracted from the susceptibility, being $\chi T \propto \xi$. This has suggested a simple linear fitting of the $\ln(\chi T)$ vs $1/T$ to evaluate the exchange contribution to the slow dynamics of SCM.[14,23b] In the case of non-collinear 1d antiferromagnets, however, the only experimentally accessible correlation is that of the *noncompensated* component of the magnetization (*b*-axis in the studied system). In fact the magnetic susceptibility cannot provide a direct estimation of the correlation of the *c* component.

In Figure 11 the solid symbols represent the experimental susceptibility $\ln(\chi_b T)$ along *b* measured in zero static field. Its linear fit as a function of $1/T$ in the low-temperature range results in $\Delta_\xi = 4.55$ K. This Δ_ξ value is much lower than $4|J|S^2 \cos \delta = 8.95$ K, and its introduction in eq 7 results in an energy barrier $\Delta = 27.9$ K for the dynamics of the magnetization, a value significantly lower than the experimental one.

Conclusions

The detailed investigation of this $[Mn(TPP)O_2PHPh]\cdot H_2O$ chain has allowed demonstrating that SCM behavior can be observed in Heisenberg AF chains provided that single ion anisotropy exceeds the exchange interaction and that the local easy axis of adjacent spins are not collinear. In other words SCM behavior is not only a feature of ferro- and ferrimagnetic but also of canted antiferromagnetic chains. The list of SCMs is therefore expected to expand as antiferromagnetic interactions are much more frequently encountered than ferromagnetic ones. Moreover, noncollinear anisotropy axes are often found in molecular systems. The larger the angle formed by the local easy axes is, the larger the uncompensated magnetic moment is. On the other side, the energy barrier for the reversal of the magnetization scales as the cosine of this angle, and thus a compromise must be found. In the case of Mn^{III} a classical treatment of the $S = 2$ spins is able to quantitatively reproduce both static and dynamics features, confirming the contributions of single ion anisotropy and isotropic exchange to the energy barrier for the reversal of the magnetization. More importantly, it has been shown that in canted AF chains it is not the correlation length extracted from susceptibility data that dominates the dynamics of the magnetization but the average length of the domains, which is significantly larger. In particular in canted AF chains the commonly employed linear analysis of $\ln(\chi T)$ vs $1/T$ leads to a large error in the estimation of the exchange contribution to the barrier. The unprecedented level of characterization of the SCM dynamics that has been reached in the investigation of this textbook example of canted antiferromagnetic chain is expected to provide a key tool to rationalize the behavior of many other single-chain magnets and to stimulate a rational synthesis of SCM with higher blocking temperatures.

Acknowledgment. We acknowledge financial support from the EC through the Human Potential Program RTN-QUEMOL-NA (FP6-504880), NE-MAGMANET (FP6-NMP3-CT-2005-515767). J.L. thanks German DFG (SPP1137) for his postdoctoral fellowship. Maria Gloria Pini, Angelo Rettori, and Dante Gatteschi are gratefully acknowledged for stimulating discussions.

Supporting Information Available: Crystallographic details in CIF format, synthetic scheme (Figure S1), crystal packing (Figures S2 and S3), angular dependence of the magnetization rotating along *a** and *b* axes (Figures S4 and S5), powder ac susceptibility (Figure S6) and the appendix reporting an extension of the Glauber model for the dynamics of canted AF chains. This material is available free of charge via the Internet at http://pubs.acs.org.

JA0751734